Chinese Journal of Chemistry, **2004**, *22*, 33—37 **Article**

Preparation and Characterization of Divanadium Pentoxide Nanowires inside SBA-15 Channels

ZHU, Ka-Ke(朱卡克) YUE, Bin*(岳斌) XIE, Song-Hai(谢颂海) ZHANG, Si-Yi(张嗣轶)
ZHANG, Biao(张飚) JIN, Song-Lin(金松林) HE, He-Yong*(贺鹤勇)

Shanghai Key Laboratory of Molecular Catalysis and Innovative Materials, Department of Chemistry, Fudan University, Shanghai 200433, China

One-dimensional V_2O_5 nanowires have been synthesized inside the channels of mesoporous silica SBA-15 through chemical approach, which involves aminosilylation of silanol groups on the silica surface, anchoring of isopoly acid, $H_6V_{10}O_{28}$, by neutralization of basic amine groups, and thermal decomposition. The formation and physicochemical properties of the nanowires were monitored and studied by TG-DTA, variable temperature *in situ* XRD, TEM, N_2 sorption measurements and UV-Vis DRS. The results indicate that V_2O_5 nanowires formed within SBA-15 channels belong to orthorhombic polycrystal domains. The oxygen-to-metal charge transfer band of V_2O_5 nanowires shows a blue shift in comparison with bulk V_2O_5, which clearly exhibits the quantum size effect of nanowires.

Keywords nanowire, mesoporous SBA-15, aminosilylation, polyoxometallate, thermal decomposition

Introduction

Recently, silica-based mesoporous materials[1] with pore size range of 2—50 nm and high surface area are of great interest as host materials for confined growing of nanoscale materials inside the channels, such as polymers,[2] metals[3] and semiconductors,[4] which have potential in catalytic,[5] environmental,[6] optoelectrical[7] and other applications. Impregnation is one of the widely used methods to introduce desired species inside the channels of mesoporous materials.[8] The method has been used to prepare Fe_2O_3, Ga_2O_3, In_2O_3, Cu_2O and $CsLaO_2$ nanoparticles inside the channels of MCM-41,[9] and Ag, Au, Pt, Pd, Rh and Si nanowires inside the channels of MCM-41, SBA-15 or HMM.[10] Another approach is based on the weak interaction between basic organic metal precursors and acidic silanol groups on the internal surface of mesoporous materials, which has been used to synthesize titania in MCM-41, zirconia in MCM-48 and rare earth oxide particles in SBA-15.[11] However, in many of these cases, uneven dispersion, poor size distribution, and weak anchoring of the loaded species often occurr.

As reported by Vansant and co-workers, the surface of silica gel may be modified with aminoalkoxysilanes,[12] resulting in the modification of acid-base property of silica surface through substituting the weak acidic silanol groups by basic amine groups. The amine groups, therefore, can be used to introduce acidic species, *e.g.* iso- and hetero-poly acid (HPA), on the internal surface of silica mesoporous materials. Iso- and hetero-poly acids containing early transition metals are well known as oxidative and acidic bifunctional catalysts in homogeneous and heterogeneous catalysis.[13] Previous report showed that,[14] by aminosilylation of silica surface of MCM-41, HPA could be immobilized inside the channels of silica mesoporous materials based on chemical bonding with amine groups, which resulted in strong anchoring of HPA and avoided its leaching in polar solvents. We speculate that in such kind of system, polyoxometallates with desired structures and compositions can be used as precursors for preparing early transition metal oxides (such as V_2O_5, MoO_3 and WO_3) and mixed oxides in the form of nanoparticles and/or nanowires. The present work investigates a simple process for introducing V_2O_5 into mesoporous SBA-15 channels by using decavanadic acid, $H_6V_{10}O_{28}$ (DVA), as a precursor. TEM, N_2 sorption, UV-Vis diffuse reflectance spectra, TG-DTA and variable temperature *in situ* XRD unambiguously confirm the formation of V_2O_5 nanowires inside SBA-15 channels. The method may be developed to prepare other early metal oxide nanowires using polyoxometallate acid as precursor.

Results and discussion

XRD

Figure 1 shows XRD patterns of SBA-15, APTS/SBA-15, and V_2O_5/SBA-15 in the 2θ range of 0.6°—10°. All samples exhibit three peaks that can be indexed as characteristic (100), (110) and (200) reflections of

* E-mail: yuebin@fudan.edu.cn and heyonghe@fudan.edu.cn; Fax: 86-21-65641740
Received April 1, 2003; revised June 23, 2003; accepted September 9, 2003.
Project supported by the National Natural Science Foundation of China (Nos. 20005310, 20371013, 20273017).

hexagonal mesoporous SBA-15, which indicates that these samples consist of well-ordered packed channels. Therefore, the primary structure of SBA-15 is maintained during aminosilylation, immobilization of DVA and formation of V_2O_5 nanowires inside the channels. The formation of V_2O_5 inside SBA-15 channels results in a rather significant decrease in the intensity of all reflections. It is probably due to pore filling of the host material[15] with V_2O_5 and a higher absorption factor of vanadium atoms for X-ray. Similar results were reported previously, some of which even showed almost no reflections of mesoporous materials in the low angle region.[11c,14] In addition, the peaks of (100), (110), and (200) reflections of APTS/SBA-15 and V_2O_5/SBA-15 slightly shifted to higher angle in comparison with those for SBA-15 (Figure 1 and Table 1), which accounts for the contraction of the host framework during surface modfication and formation of V_2O_5 nanowires inside the channels by calcination.

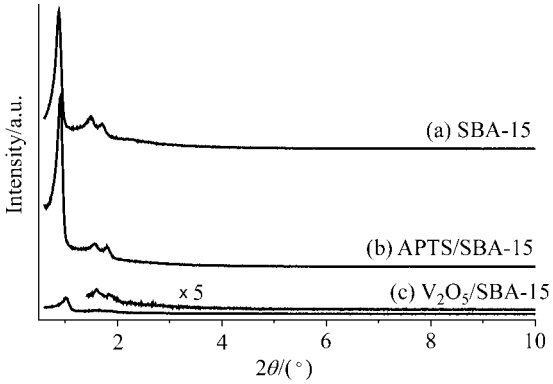

Figure 1 Low-angle XRD patterns of (a) SBA-15, (b) APTS/SBA-15 and (c) V_2O_5/SBA-15.

TG-DTA and variable temperature *in situ* XRD

TG-DTA and variable temperature *in situ* XRD patterns of DVA/APTS/SBA-15 and bulk V_2O_5 are shown in Figures 2 and 3, respectively. The TG curve of DVA/APTS/SBA-15 displays a weight loss of 4.5% in the region of 150—380 ℃ in succession, which is due to oxidation of organics and decomposition of DVA. There is no noticeable weight loss above 380 ℃. The DTA curve also exhibits a broad exothermic peak at 261 ℃ and a small exothermic peak at 372 ℃, which indicates that the organics have been totally removed and the decomposition of DVA to form V_2O_5 has been completed below 380 ℃. The temperature of the endothermic peak at 627 ℃ is slightly lower than the melting point of bulk V_2O_5. XRD pattern in Figure 3a shows that DVA immobilized sample displays no characteristic reflections of DVA, indicating no crystalline DVA inside or outside of SBA-15 channels. The hump centered

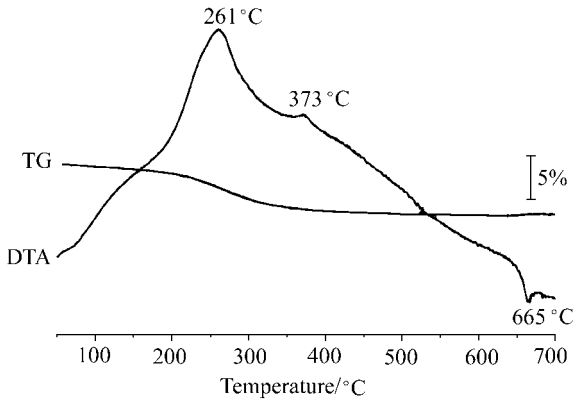

Figure 2 TG-DTA plots of APTS/DVA/SBA-15.

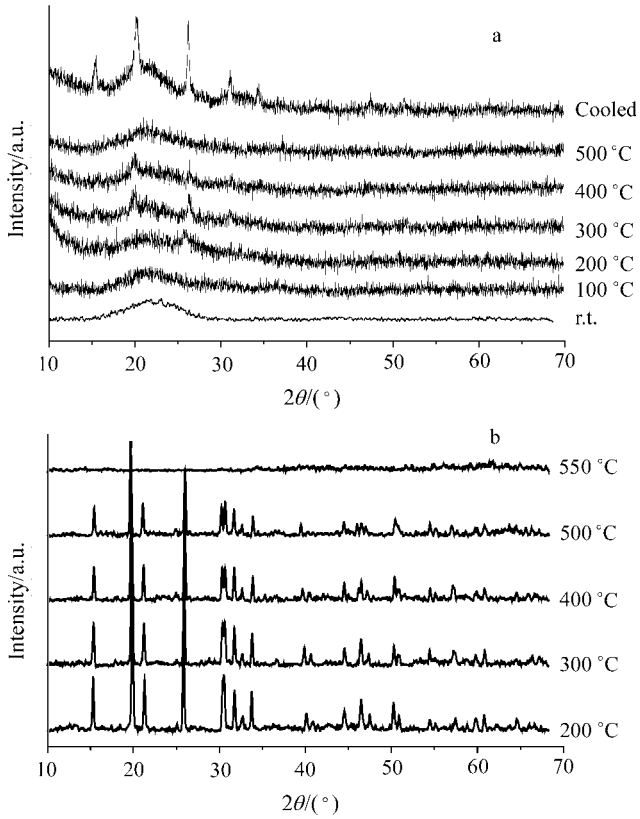

Figure 3 Variable temperature *in situ* XRD patterns of (a) DVA/APTS/SBA-15 and (b) V_2O_5.

Table 1 XRD data and porous properties of SBA-15 and its modified samples

Sample	d_{hkl}/nm			Surface area/($m^2 \cdot g^{-1}$)	Pore diameter/nm	Pore volume/($cm^3 \cdot g^{-1}$)
	d_{100}	d_{110}	d_{200}			
SBA-15	10.04	5.929	5.196	674.3	7.78	1.25
APTS/SBA-15	9.816	5.663	4.908	333.7	6.72	0.639
V_2O_5/SBA-15	9.299	5.521	4.827	269.9	6.47	0.435

at *ca.* 24° comes from the diffraction of the amorphous framework of SBA-15. The decomposition of DVA into V_2O_5 takes place between 200—400 ℃ with appearance of pure characteristic orthorhombic phase of V_2O_5 with lattice constants a=1.1516 nm, b=0.35656 nm and c=0.43727 nm (JCPDS 41-1426). The orthorhombic structure of V_2O_5[16] has an anisotropic layered structure, which consists of distorted trigonal bipyramids of VO_5 sharing edges to form zigzag double chains. When the sample is heated between 300 and 400 ℃, (200), (001), (110) and (400) reflections of crystalline V_2O_5 can be observed, which confirms that decomposition of DVA occurs concomitantly during oxidation of the organics. These reflections disappear when temperature is above 400 ℃ and re-appear during cooling. Although the same trend can be observed from bulk V_2O_5, bulk V_2O_5 appears more thermally stable than the crystalline V_2O_5 nanowires as the reflections of the former still appear at 500 ℃ (Figure 3b). This indicates, as a quantum-sized effect, that the thermal vibration energy of the atoms in nanoscale V_2O_5 lattice is high enough to deform the crystal structure at lower temperature.

TEM and HRTEM

All micrographs are recorded with the electron beam direction nearly parallel to and perpendicular to the channel direction. TEM images in Figures 4a and 4b show that the highly ordered mesoporous structure of SBA-15 remains after the formation of V_2O_5 nanowires inside the SBA-15 channels. As shown in Figure 4c, HRTEM image further supports the formation of the V_2O_5 nanowires. Although the image of nanowires of V_2O_5 appears slightly unclear due to covering of the amorphous silica walls, it is still obvious that the V_2O_5 nanowires located inside the channels of SBA-15 are crystalline and the growth orientations of nanowires are different. The observed d spacings of 0.56 and 0.35 nm are attributed to (200) and (010) planes, respectively, which is consistent with the *in situ* XRD results. EDX provides a molar ratio of 11.7 for Si/V, indicating *ca.* 11 wt% of V_2O_5 loading. The nanoscale materials are generally easy to sinter when they are thermally treated, unless their growth is somewhat confined.[17] In the present case, the limited space of SBA-15 channels restricts the sinter of V_2O_5 nanowires. Therefore, the nanostructure of V_2O_5 inside the channels can be kept even after calcination at 500 °C for 3 h.

N_2 sorption

Figure 5 shows the N_2 adsorption-desorption isotherms of SBA-15, APTS/SBA-15 and V_2O_5/SBA-15. The isotherm of SBA-15 is of Type IV classification, which has typical hysteresis loop of mesoporous materials.[18] The surface modified sample, APTS/SBA-15, and the nanowires containing sample, V_2O_5/SBA-15, retain the same shape of isotherm. However, the amount of adsorbed nitrogen decreases and the onset of the capillary condensation step shifts to relative lower pressures. The decrease of the amount of adsorbed N_2 can be attributed to the reduced pore volume and the condensation in adsorption branch starting at lower p/p_0 is caused by the smaller pore size. Both are confirmed by the data in Table 1. The filling of the channels after aminosilylation and formation of V_2O_5 nanowires accounts for the decrease of the pore volume, pore size and surface area. Nevertheless, it should be noted that the hysteresis in the high-pressure range of p/p_0=0.5—0.6 corresponds to the mesoporosity of SBA-15,[19] confirming that V_2O_5 nanowires are located inside the channels and the mesoporous channels still remain.

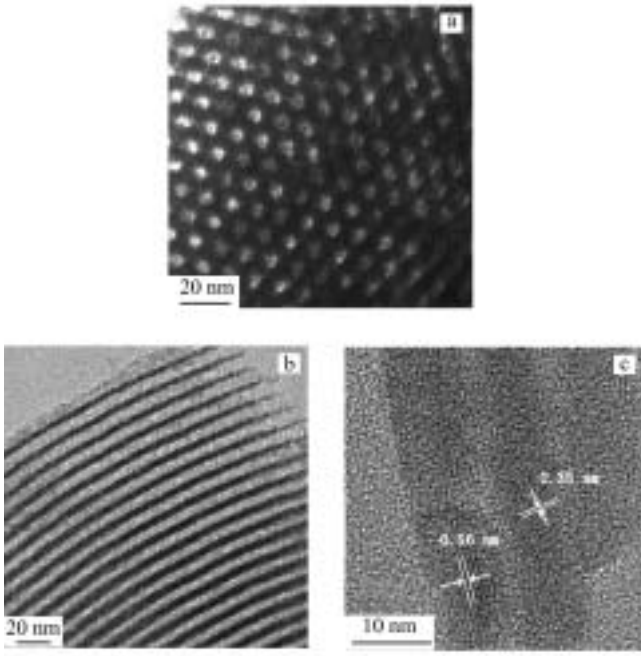

Figure 4 TEM images of the V_2O_5/SBA-15 sample (a) taken with the beam direction parallel to the pores and (b) taken with the beam direction perpendicular to the pores. (c) HRTEM image of the crystalline V_2O_5 nanowires in SBA-15 with different growth orientations along the wire directions. The *d* spacings of 0.56 and 0.35 nm are attributed to (200) and (010) planes, respectively.

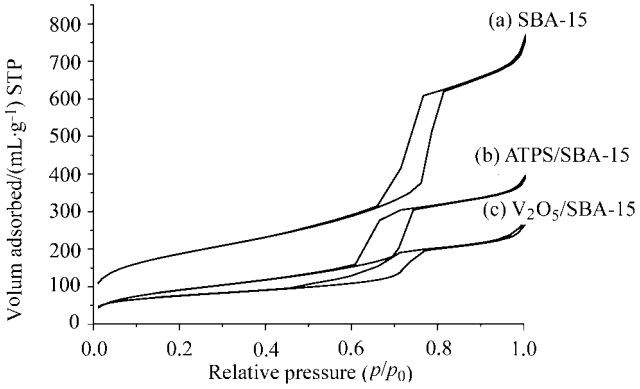

Figure 5 Nitrogen adsorption-desorption isotherms of (a) SBA-15, (b) APTS/SBA-15, and (c) V_2O_5/SBA-15.

UV-vis DRS

The UV-vis diffuse reflectance spectra of SBA-15, V_2O_5/SBA-15 and V_2O_5 are shown in Figure 6. SBA-15 displays very little absorption. Two main absorption bands are presented at 333 and 472 nm in bulk V_2O_5, which are assigned to low energy oxygen-to-metal charge transfer bands. In V_2O_5/SBA-15 the absorption bands shift to 304 and 365 nm and the absorption edge is less steep in comparison with that of bulk V_2O_5. The blue-shift of the absorption bands reflects the quantum size effect.[4a,20]

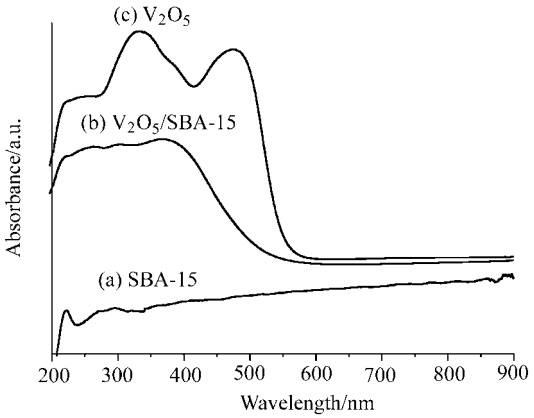

Figure 6 UV-vis diffuse reflectance spectra of (a) SBA-15, (b) V_2O_5/SBA-15 and (c) V_2O_5.

In conclusion, crystalline nanowires of transition metal oxides V_2O_5 have been successfully prepared using mesoporous silica SBA-15 as template through aminosilylation and subsequent anchoring of decavanadic acid, $H_6V_{10}O_{28}$, followed by thermal decomposition. The characterization results indicate that the crystalline V_2O_5 nanowires form in the channels of SBA-15 with different growth orientations. The current process represents a useful approach for synthesizing metal oxide nanowires using polyoxometallate acid as precursor, which may be applied for selective anchoring of desired species to form nanoscale host-guest materials.

Experimental

Preparation of SBA-15

SBA-15 was synthesized in acidic conditions using the tri-block copolymer, poly(ethylene oxide)-poly(propylene oxide)-poly(ethylene oxide) ($EO_{20}PO_{70}EO_{20}$) (Aldrich), as template and tetraethyl orthosilicate (TEOS, 98%, Aldrich) as a silicon source.[21] A solution of $EO_{20}PO_{70}EO_{20}$ ∶ HCl (2 mol • L^{-1}) ∶ TEOS ∶ H_2O = 2 ∶ 60 ∶ 4.25 ∶ 15 (mass ratio) was prepared, stirred for 4 h at 40 ℃, and then heated at 95 ℃ for 3 d. The solid products were filtered and calcinated at 550 ℃ for 4 h. Before grafting reaction, samples were dried at 180 ℃ for 3 h *in vacuo*.

Aminosilylation of SBA-15 channel surface

Aminosilylation reaction was performed according to the reported literature method[14] with minor modification. In a typical preparation, 1 g of SBA-15 was refluxed in a 30 mL of toluene solution containing 1% (*V/V*) γ-aminopropyltriethoxysilane (APTS) for 5 h. The resulting material, denoted as, was filtered, washed with toluene, and dried at 95 ℃ for 3 h to remove the remaining solvent.

Immobilization of DVA inside APTS/SBA-15

The aqueous solution of DVA was prepared by exchange of an aqueous solution of $(NH_4)_6V_{10}O_{28}$[22] through acidic ion exchange resin. To immobilize DVA in modified SBA-15 channels, 1 g of APTS/SBA-15 was stirred in a 30 mL of aqueous solution containing 5.5×10^{-4} mol of DVA at 60 °C for 8 h. The resulting solid, denoted as DVA/APTS/SBA-15, was filtered and washed with methanol three times to remove the unanchored DVA, and dried at 95 °C for 3 h.

Formation of V_2O_5 nanowires inside SBA-15 channels

DVA/APTS/SBA-15 was further achieved by temperature programmed thermal decomposition from 95 to 500 °C at 2 °C/min and finally calcinated at 500 °C for 5 h in air. The product is denoted as V_2O_5/SBA-15. The whole procedure is shown in Scheme 1.

Scheme 1

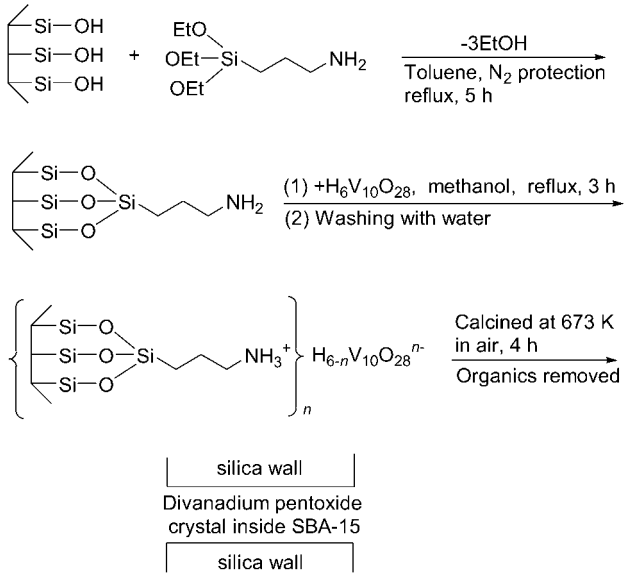

Characterization

X-ray diffraction patterns were recorded on a Bruker D8 Advanced X-ray diffractometer using Cu Kα radiation, with a voltage of 40 kV and a current of 40 mA. Variable temperature *in situ* XRD experiments were carried out on the same diffractometer from 100 to 600 ℃ at a speed of 0.2 ℃/s. TG-DTA results were obtained on a Perkin Elmer TGA7 thermogravimetric analyzer. The average pore size, pore volume and BET surface area were determined by N_2 adsorption-desorption measurement at 77 K on a Micromeritics Tristar 3000 analyzer. The pore size distribution was calculated

from the desorption branch of the isotherms by BJH method. Transmission electron microscopy (TEM) was performed using a Joel JEM-2010 transmission electron microscope. Elemental maps were obtained by analysis of the K-edge fluorescence for Si and V. UV-Vis diffuse reflectance spectra (DRS) in the wavelength region of 190—900 nm were recorded on a JASCO V-570 UV/VIS/NIR spectrophotometer.

References

1 Ciesla, U.; Schüth, F. *Microporous Mesoporous Mater.* **1999**, *27*, 131.

2 (a) Feng, Q. W.; Xu, J. G.; Dong, H.; Li, S. X.; Wei, Y. *J. Mater. Chem*. **2000,** *10*, 2490.
(b) Spange, S.; Graser, A.; Huwe, A.; Kremer, F.; Tintemann, C.; Behrens, P. *Chem.-Eur. J.* **2001**, *7*, 3722.
(c) Maki-Ontto, R.; de Moel, K.; de Odorico, W.; Ruokolainen, J.; Stamm, M.; ten Brinke, G.; Ikkala, O. *Adv. Mater.* **2001**, *13*, 117.

3 (a) Huang, M. H.; Choudrey, A.; Yang, P. *Chem. Commun.* **2000**, 1063.
(b) Plyuto, Y.; Berquier, J. M.; Jacquiod, C.; Ricolleau, C. *Chem. Commun.* **1999**, 1653.

4 (a) Gao, F.; Lu, Q.; Liu, X.; Yan, Y.; Zhao, D. *Nano Lett.* **2001**, *1*, 743.
(b) Zhang, W.-H.; Shi, J.-L.; Chen, H.-R.; Hua, Z.-L.; Yan, D.-S. *Chem. Mater.* **2001**, *13*, 648.
(c) Stucky, G. D.; MacDougall, J. E. *Science* **1990**, *247*, 669.

5 (a) Wingen, A.; Anastasievic, N.; Hollnagel, A.; Werner, D.; Schüth, F. *J. Catal*. **2000**, *193*, 248.
(b) Kim, S. W.; Son, S. U.; Lee, S. I.; Heyon, T.; Chung, Y. K. *J. Am. Chem. Soc.* **2000**, *122*, 1550.

6 Feng, X.; Fryxell, G. E.; Wang, L. Q.; Kim, A. Y.; Liu, J.; Kemner, K. M. *Science* **1997**, *276*, 923.

7 (a) Yang, P.; Wirnsberger, G.; Huang, H. C.; Cordero, S. R.; McGehee, M. D.; Scott, B.; Deng, T.; Whitesides, G. M.; Chmelka, B. F.; Buratto, S. K.; Stucky, G. D. *Science* **2000**, *287*, 465.
(b) Chakraborty, P. *J. Mater. Sci*. **1998**, *33*, 2235.

8 Kloetstra, K.; Van Bekkum, H. *Stud. Surf. Sci. Catal.* **1997**, *105*, 431.

9 (a) Fröba, M.; Köhn, R.; Bouffaud, G.; Richard, O.; Van Tendeloo, G. *Chem. Mater*. **1999**, *11*, 2858.
(b) Choudhary, V. R.; Jana, S. K.; Kiran, B. P. *J. Catal*. **2000**, *192*, 257.

10 (a) Han Y. J.; Kim, J. M.; Stucky, G. D. *Chem. Mater*. **2000**, *12*, 2068.
(b) Fukuoka, A.; Sakamoto, Y.; Guan, S.; Inagaki, S.; Sugimoto, N.; Fukushima, Y.; Hirahara, K.; Iijima, S.; Ichikawa, M. *J. Am. Chem. Soc*. **2001**, *123*, 3373.
(c) Coleman, N. R. B.; Morris, M. A.; Spalding, T. R.; Holmes, J. D. *J. Am. Chem. Soc*. **2001**, *123*, 187.

11 (a) Zheng, S.; Gao, L.; Zhang, Q. H.; Guo, J. K. *J. Mater. Chem*. **2000**, *10*, 723.
(b) Morey, M. S.; Stucky, G. D.; Schwarz, S.; Fröba, M. *J. Phys. Chem. B* **1999,** *103*, 2037.
(c) Sauer, J.; Marlow, F.; Spliethoff, B.; Schüth, F. *Chem. Mater*. **2002**, *14*, 217.

12 van der Voort, P.; Vansant, E. F. *J. Liq. Chromatogr. Relat. Technol*. **1996**, *19*, 2723.

13 Kozhevnikov, I. V. *Chem. Rev*. **1998**, *98*, 171.

14 Kaleta, W.; Nowińska, K. *Chem. Commun*. **2001**, 535.

15 Marler, B.; Oberhagemann, U.; Vortmann, S.; Gies, H. *Microporous Mater*. **1996**, *6*, 375.

16 Bachmann, H. G.; Ahmes, F. R.; Barnes, W. H. *Zeit. Krist*. **1961**, *115*, 110.

17 Zhang, W.-H.; Shi, J.-L.; Wang, L.-Z.; Yan, D.-S. *Chem. Mater*. **2000**, *12*, 1408.

18 Sing, K. S. W.; Everett, D. H.; Haul, R. A. W.; Moscou, L.; Pierotti, R. A.; Rouquérol, J.; Siemieniewska, T. *Pure Appl. Chem*. **1985**, *57*, 603.

19 Kruk, M.; Jaroniec, M.; Sakamoto, Y.; Terasaki, O.; Ryoo, R.; Ko, C. H. *J. Phys. Chem. B* **2000**, *104*, 292.

20 Sooklal, K.; Cullum, B. S.; Angel, S. M.; Murphy, C. J. *J. Phys. Chem*. **1996**, *100*, 4551.

21 Zhao, D.; Feng, J.; Huo, Q.; Melosh, N.; Fredrickson, G. H.; Chemlka, B. F.; Stuky, G. D. *Science* **1998**, *279*, 548.

22 Johnson, G. K.; Murmann, R. K. *Inorg. Synth*. **1979**, *19*, 140.

(E0304012 LI, L. T.)